

## Article

# Geochronology, Petrogenesis, and Tectonic Setting of the Late Triassic Banpo Pluton from the Western Part of the North Qinling Orogenic Belt

Shuqin Li <sup>1</sup>, Zuochen Li <sup>1,2,\*</sup> , Xianzhi Pei <sup>1,2</sup>, Hao Lin <sup>1</sup>, Li Qin <sup>1</sup>, Shang Ji <sup>1</sup>, Yajie Yang <sup>1</sup> and Jinghong Ren <sup>1</sup>

<sup>1</sup> Key Laboratory of Western China's Mineral Resources and Geological Engineering, Ministry of Education, School of Earth Science and Resources, Chang'an University, Xi'an 710054, China; 18706793100@163.com (S.L.); peixzh@chd.edu.cn (X.P.); linhao231@163.com (H.L.); qinlichd@163.com (L.Q.); chdj2022@163.com (S.J.); yangyajie202211@163.com (Y.Y.); 18534768748@163.com (J.R.)

<sup>2</sup> Xi'an Key Laboratory for Mineralization and Efficient Utilization of Critical Metals, Xi'an 710054, China

\* Correspondence: lizuochen@chd.edu.cn

**Abstract:** Precise determination of the tectonothermal events at the Qinling–Qilian junction is significant for understanding the tectonic evolution of the eastern branch of the Paleo-Tethys. The Banpo pluton outcrops in the northern margin of the North Qinling were chosen as the research subject and their formation and tectonic environment were investigated using zircon U–Pb age and geochemical compositions. The weighted average values of <sup>206</sup>Pb/<sup>238</sup>U ages of samples from three sites of the Banpo pluton corresponded to 213.4 ± 2.1 Ma (MSWD = 0.56), 213.0 ± 1.6 Ma (MSWD = 0.92), and 216.3 ± 2.3 Ma (MSWD = 2.0). All the samples are rich in light rare earth elements, exhibiting a seagull-type right-leaning partitioning curve, with obviously negative Eu anomalies. In addition, based on the regional geological data, it can be concluded that the Banpo pluton was formed during the transition period from a post-Orogenic environment to an anorogenic environment. The results indicated the final stage of the Triassic orogeny and the closure phase of the Paleo-Tethys. Also, it shows closure of the Paleo-Tethys–Mianxian–Lueyang Ocean by the Late Triassic period as well as the completion of the collision between the North China and Yangtze Blocks along the Qinling Orogenic Belt.

**Keywords:** North Qinling Orogenic Belt; Late Triassic; tectonic setting; petrogenesis; geochronology; syenitic porphyries



**Citation:** Li, S.; Li, Z.; Pei, X.; Lin, H.; Qin, L.; Ji, S.; Yang, Y.; Ren, J. Geochronology, Petrogenesis, and Tectonic Setting of the Late Triassic Banpo Pluton from the Western Part of the North Qinling Orogenic Belt. *Minerals* **2024**, *14*, 222. <https://doi.org/10.3390/min14030222>

Academic Editor: Rubén Díez-Fernández

Received: 20 December 2023

Revised: 10 February 2024

Accepted: 12 February 2024

Published: 22 February 2024



**Copyright:** © 2024 by the authors. Licensee MDPI, Basel, Switzerland. This article is an open access article distributed under the terms and conditions of the Creative Commons Attribution (CC BY) license (<https://creativecommons.org/licenses/by/4.0/>).

## 1. Introduction

The conjunction area between the Qinling Orogenic Belt and the Qilian Orogenic Belt is the key section for connecting the Central Orogenic Belt of China from east to west (Figure 1a). It is located at the intersection of the Tethyan tectonic domain and the Paleo-Asian tectonic domain and it serves as a convergence junction for several blocks and the Orogenic Belt [1–6]. The Indosinian Qinling Orogenic Belt exhibits intense magmatic activity, leading to the formation of volcanic plutonic rocks, particularly, Indosinian granite, diorite, and other intermediate-acid rocks [7]. These magmatic events not only serve as important records of complex subduction–collision orogeny in the Mesozoic [6,8–10] but also characterize the deep dynamic mechanism and provide significant insights into the geological structure evolution of the Central Orogenic Belt of China [9,11,12]. Furthermore, they are closely associated with the opening and closing processes of the Mianxian–Lueyang Ocean [13–15]. The evolution of the Paleo-Tethys Ocean, as a significant geological event in the global sea land pattern changes since the late Paleozoic era, has always been a frontier and hot topic in domestic and foreign research on the definition and spatiotemporal evolution process of the Paleo-Tethys tectonic domain [16]. Research has shown that the collision between the subduction accretion system and the banded terrain caused by the

closure of the Paleo-Tethys ocean basin ultimately formed the Paleo-Tethys Orogenic system through arc–continent collision and continent–continent collision [17].

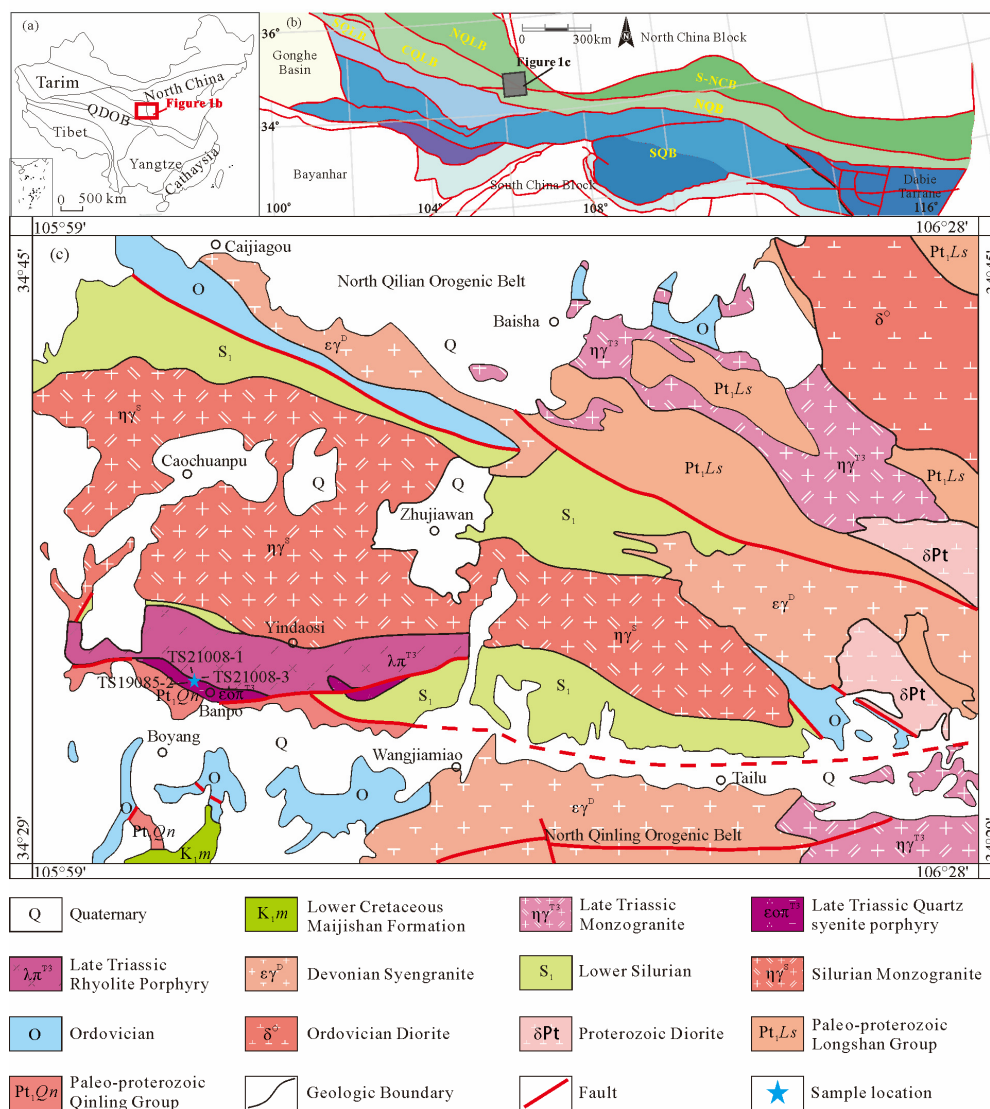


**Figure 1.** (a) Geotectonic map of China. (b) Map showing the regional context of the West Qinling Orogenic Belt (WQOB); the North Qilian Belt (NQLB); the southern margin of the North China Block (S-NCB); the Central Qilian Belt (CQLB); the North Qinling Belt (NQB); the South Qinling Belt (SQB); geological map modified from Dong et al. [6]. (c) Map showing the regional geological makeup of the Banpo pluton in the North Qinling Belt, geological map after Xu et al. [18].

The early and late phases of the Indosinian period are characterized by varying distribution and spreading of the main intrusive rocks formed during those phases. The early intrusive rocks are located in the central and western parts of the southern region of the North Qinling Orogenic Belt and exhibit a north–south reverse-strip distribution, which aligns with the regional tectonic lines. The late Indosinian intrusive rocks are primarily distributed in the central southern part of the North Qinling Orogenic Belt [8,9,19–26]. In recent years, several researchers have studied the Indosinian intrusive rocks found in the western region of the North Qinling Belt and proposed different perspectives on the formation of the tectonic environment, categorizing them into the early subduction stage and late-collision or post-collision stage [2,27–36]. Regionally, the granite in the Western Qinling Mountains is mainly developed on the northern side of the Xiahe Hezhe Lintan Minxian Dangchang fault and is mainly of the Indosinian period. Based on the basic facts of

the Banpo intrusion studied in this article, combined with the reports of Xu Xueyi et al. on the Zhongchuan and Wenquan plutons on the western side of the region [20], it is indicated that a crustal thickening event occurred in the late Permian Triassic period in the study area, which may be a composite tectonic event, including the collision between the Yangtze Plate and the North China Plate and the subduction in the northern part of the ancient Tethys Basin.

Understanding the genesis of granitic rocks, especially A-type granites, is essential for comprehending the tectonic formation and evolution of the continental crust. It also provides a novel concept for examining the underlying genetic mechanism and deep dynamic background of collision-type magmatic rocks in the Orogenic Belt [37–48]. This study has selected the Banpo pluton outcrops in the western section of the North Qinling Orogenic Belt to determine its formation age and evaluate its significance in the geological evolution of the western section of the North Qinling Orogenic Belt through detailed field investigation, geochronology, petrology, and geochemical studies.

## 2. Geological Background

The Qinling Orogenic Belt is a composite continental collision Orogenic belt consisting of two major suture zones, namely, the Shangdan Belt and the Mianlue Belt, and three blocks, namely, the southern margin of the North China Block, the Qinling Micro-Block, and the northern margin of the Yangtze Block (Figure 1b) [6]. It is in contact with the Paleoproterozoic Qinling Group and the Meso- to Neoproterozoic Huluhe Group to the south in a fault intrusion relationship and a small amount of dark-colored microgranular enclaves can be observed within the porphyry body, with a particle size of approximately 10 cm. To the north, it is in intrusive contact with the Xiaohezi volcanic rock body and existing studies have shown that the Xiaohezi volcanic rocks were formed during the late Indosinian period [19]. The Banpo pluton is intrusively emplaced within the Indosinian period Xiaohezi volcanic rocks, indicating that they are roughly contemporaneous products (Figure 1c) [48].

## 3. Petrography

The Banpo pluton is primarily a flesh-red, medium-coarse-grained porphyritic syenite with prominent flesh-red outcrops (Figure 2a,b). It consists of medium-coarse granitic, porphyritic, and massive structures. The Banpo pluton is mainly composed of plagioclase, quartz, a small amount of potassium feldspar, biotite, magnetite, sphene, and zircon. The orthoclase is hypidiomorphic, with a grain size ranging from 0.07 mm × 0.22 mm to 0.1 mm × 0.3 mm and a content of 50%–60%. It forms simple twin crystals and visible stripe structures, with potassium feldspar creating a ring-shaped structure around quartz (see Figure 2c). The phenocrysts are predominantly composed of orthoclase with a small amount of plagioclase. The orthoclase crystals exhibit hemidiomorphic–idiomorphic shapes, with both Carlsbad and lattice twin crystals, characterized by long columns and plates (approximately 0.6–1.0 cm long). Its content ranges from about 15%–30%, with the maximum varying between 35% and 40%. In the matrix, the components are mainly composed of plagioclase, potassium feldspar, a small amount of biotite, amphibole, and so on. Plagioclase ranges from 0.5 mm to 2.5 mm in size and occurs as grayish white subhedral columnar with polysynthetic twinning, with a content of 5%–10% (see Figure 2d). Biotite is partially altered to chlorite or epidote and occurs as irregular scaly or short columnar shapes, measuring between 0.5 mm and 2.5 mm in size.

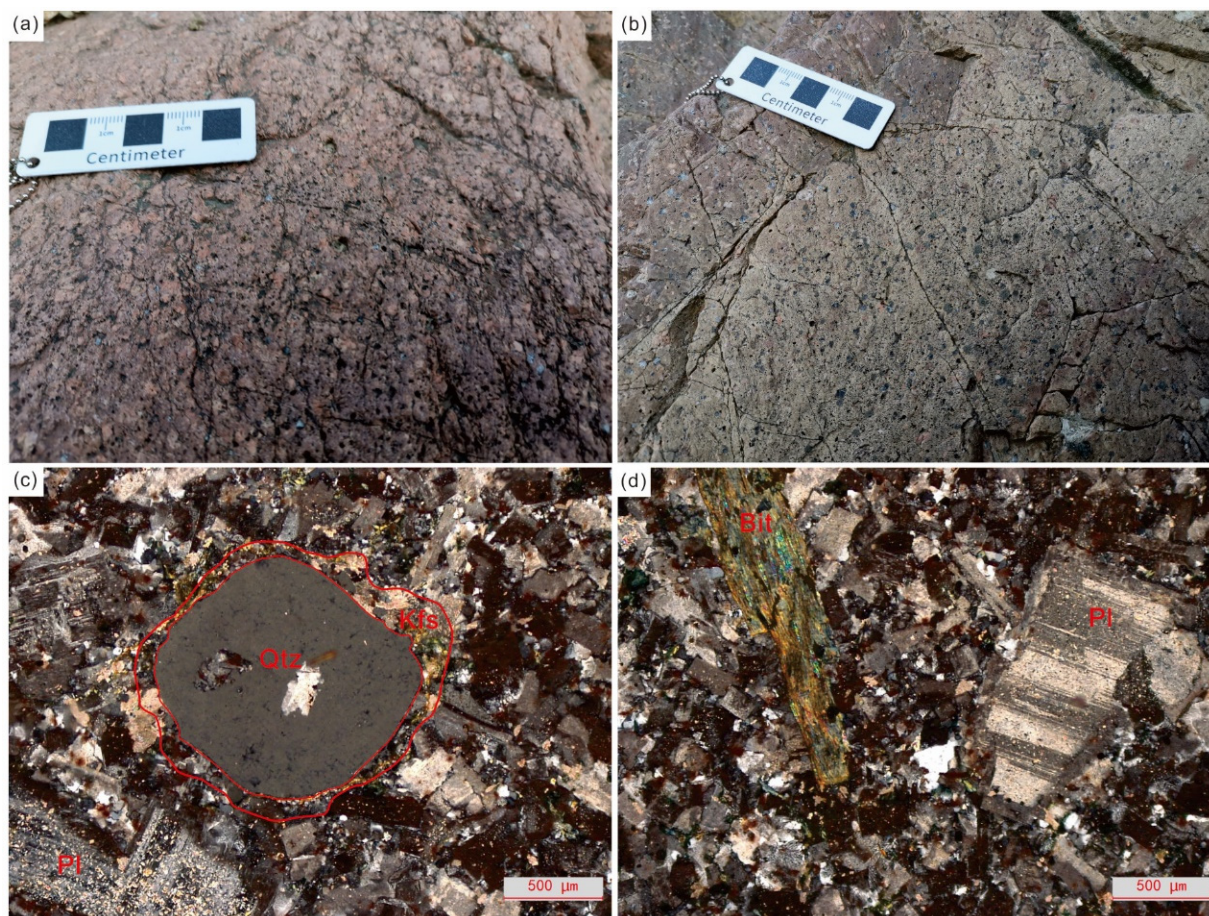


**Figure 2.** Field photographs and photomicrographs of the Banpo pluton in the western section of the North Qinling Orogenic Belt (WNQOB). (a,b) Field photographs of the Banpo pluton; and (c,d) photomicrographs of the Banpo pluton. Mineral abbreviations are as follows: Qtz = quartz, Pl = plagioclase, Bit = biotite, and Kfs = K-feldspar.

#### 4. Analytical Methods

##### 4.1. Zircon U-Pb Geochronology

Zircon U-Pb dating was performed on three samples (TS21008-1, TS21008-3, and TS19085-2) from the Banpo pluton. The locations of the three samples are  $34^{\circ}33'47''$  N,  $106^{\circ}03'56''$  E,  $34^{\circ}33'50''$  N,  $106^{\circ}03'57''$  E, and  $34^{\circ}33'43''$  N,  $106^{\circ}03'55''$  E. The samples were crushed and sorted at Xi'an Ruishi Geological Technology Co., Ltd. Subsequently, transreflectance and cathodoluminescence (CL) imaging techniques were used to analyze the microscopic structure of the zircon grains. The optimal zircon domains suitable for U-Pb isotope dating were identified. The zircon separation work mentioned in this study was performed at Xi'an Ruishi Geological Technology Co., Ltd. (Xi'an Ruishi Geological Technology Co., Ltd., Xi'an, China). The zircon targets and cathodoluminescence (CL) images were provided by Beijing Geoanalysis Co., Ltd., Beijing, China. The zircon U-Pb isotope analysis was performed using laser ablation multi-collector inductively coupled plasma mass spectrometry (LA-MC-ICP MS) at Beijing Geoanalysis Co., Ltd., Beijing, China. The laser denudation system used is GeoLas 2005 and the ICP-MS is Agilent 7500a. The ICP-MS used for zircon dating is Agilent 7500a produced by Agilent (Santa Clara, CA, USA). Helium was used as carrier gas, the laser beam spot diameter was  $32\ \mu\text{m}$ , the denudation depth was  $20\text{--}40\ \mu\text{m}$ , and the laser pulse was 8 Hz. The international standard zircon sample of 91,500 was used as an external standard for the calculation of zircon ages. The artificial synthetic silicate glass NIST610 [49], American National Standard Substance Bureau, was adopted as an external standard for element content analysis.  $^{29}\text{Si}$

was used as the internal standard element. The isotopic ratio and element content data were analyzed using the ICPMS Data Cal software package [50]. The raw data obtained from the test was processed and corrected using ICPMS Data Cal 11.1 software [51]. The general lead adjustment was conducted using Andersen software [52] and Isoplot software (3.0 edition) [53] was used for age calculation and concordia diagrams. The analytical methods and instrument settings used were the same as those reported by Vermeesch [54].

#### 4.2. Geochemical Analyses

Fourteen samples were selected for major and trace element analyses. Major and trace elements were measured at the Langfang Fengzeyuan Rock and Mineral Detection Technology Co., Ltd. (Langfang, China). All samples were broken to less than 200 mesh. The major element test was performed by wavelength dispersive ray fluorescence spectrometer (XRF) and the analysis error was analyzed. More details can be found in Ma et al. [55]. For the major element analysis, the sample was initially determined for loss on ignition and, then, melted into glass sheets. The analytical accuracy of the Shimadzu 1800 X-ray fluorescence spectrometer was around 2%. The trace and rare earth elements (REEs) were analyzed by the ICP-MS (Thermo-X7, Thermo Fisher Scientific, Waltham, MA, USA). Samples were prepared using the acid-solubility method, which has an analytic precision of >10%, according to national standards GSR-1 (GBW07103) and GSR-3 (GBW07105). However, the precision is >5% when element content is >10 ppm.

### 5. Results of Analyses

The zircon U-Pb isotope data and whole-rock geochemistry for the Banpo pluton are listed in Supplementary Tables S1–S3.

#### 5.1. Zircon U-Pb Age and REE Geochemistry

The zircons of Banpo pluton are colorless and transparent, with grain sizes between ~100  $\mu\text{m}$  and 200  $\mu\text{m}$ . The crystals have columnar and long columnar shapes and develop into magmatic crystallization belts. The CL images and measurement points of some typical zircons are shown in Figure 3 [56–58].

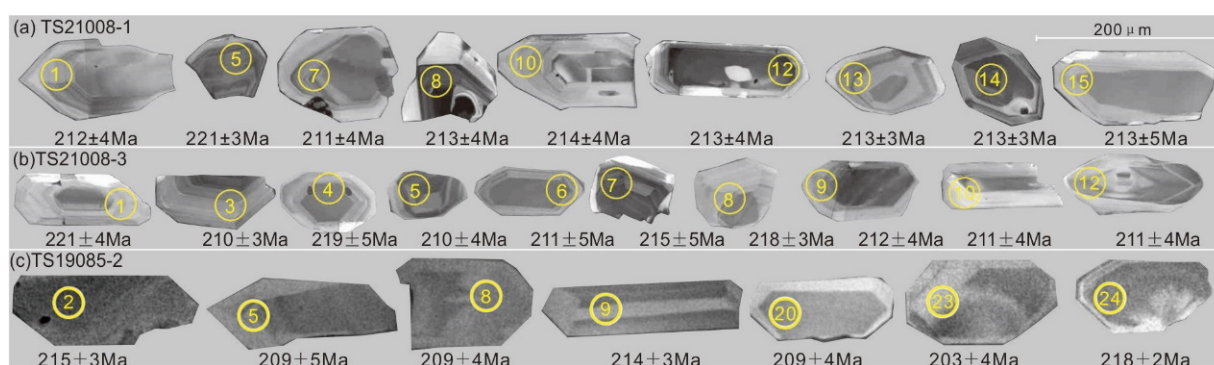


**Figure 3.** CL images and single-zircon  $^{206}\text{Pb}/^{238}\text{U}$  ages of zircons of the Banpo pluton in the western section of the North Qinling Orogenic Belt: (a) sample TS21008-1; (b) sample TS21008-3; and (c) sample TS19085-2.

The Th content of TS21008–1 zircon ranged from 66.99 ppm to 547.76 ppm, whereas the U content ranged from 90.37 ppm to 926.55 ppm. The Th/U ratio ranged from 0.38 to 0.98 and the majority of the Th/U ratios exceeded 0.4 and the Th and U are positively correlated. The distribution pattern of REEs demonstrates a left-leaning curve of heavy rare earth enrichment (HREE) with negative Eu and positive Ce anomalies (Figure 4a) (Supplementary Table S1). U-Pb isotope age analysis was performed on 25 zircons sampled from Banpo pluton and 25 points were determined (Supplementary Table S2). Excluding nine data values with harmonicity less than 90% and significantly higher age values, the

remaining  $^{206}\text{Pb}/^{238}\text{U}$  age values ranged from 205 to 221 Ma. The weighted average age of  $^{206}\text{Pb}/^{238}\text{U}$  corresponds to  $213.4 \pm 2.1$  Ma, with MSWD = 0.56 (Figure 5a,b).

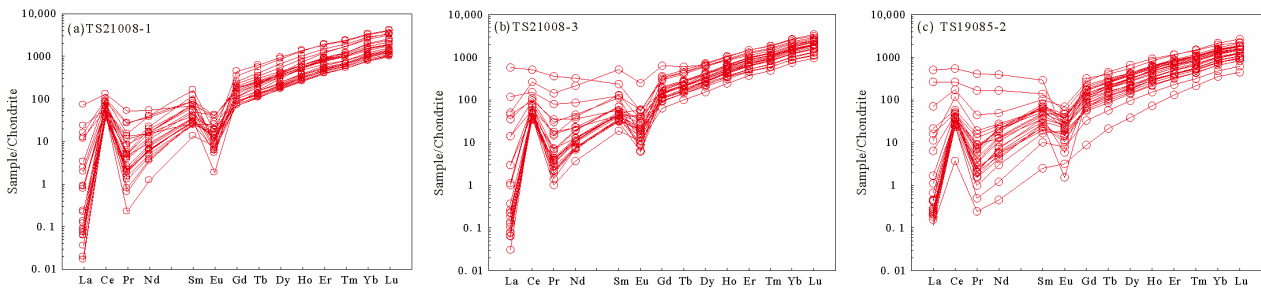


**Figure 4.** Chondrite–normalized rare earth element (REE) patterns in the zircon grains of the Banpo pluton in the western section of the North Qinling Orogenic Belt: (a) sample TS21008-1; (b) sample TS21008-3; and (c) sample TS19085-2.

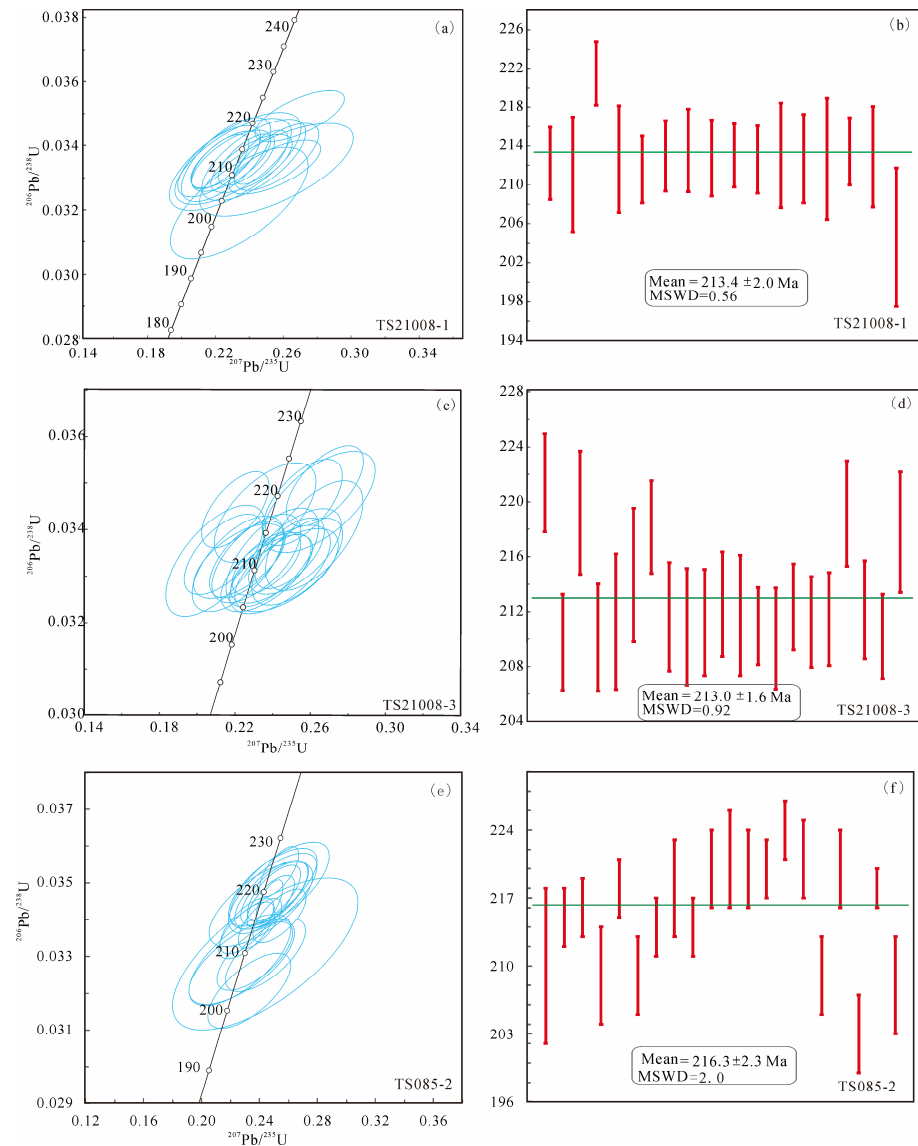


**Figure 5.** LA–ICP–MS zircon U–Pb concordia diagram and weighted average age diagram of zircons of the Banpo pluton in WNQOB: (a,b) sample TS21008-1; (c,d) sample TS21008-3; and (e,f) sample TS19085-2.

The Th content of TS21008–3 zircon ranged from 83.50 ppm to 397.48 ppm, whereas the U content ranged from 131.61 ppm to 607.86 ppm. The Th/U ratio ranged between 0.44 and 4.06 and the majority of the Th/U ratios exceeded 0.4. The positive correlation between Th and U indicates the magmatic origin of zircon. The distribution pattern of REEs demonstrates a left-leaning curve of HREE type, indicating negative Eu and positive Ce anomalies (Figure 4b) (Supplementary Table S1). U-Pb isotope age analysis was performed on 25 zircons sampled from Banpo pluton and 25 points were determined (Supplementary Table S2). After the exclusion of four data points with a concordance below 90%, the remaining  $^{206}\text{Pb}/^{238}\text{U}$  age values ranged from 210 to 221 Ma. A majority of the zircon data points aligned with the concordant diagram are at or near the concordant line, while a few zircon data points deviated from the concordia. The possible reason for the deviation of data points can be attributed to the initial loss of common Pb in the zircon. However, this did not lead to a significant effect on the accuracy of  $^{206}\text{Pb}/^{238}\text{U}$  age estimates. The weighted average age value of  $^{206}\text{Pb}/^{238}\text{U}$  corresponds to  $213.0 \pm 1.6$  Ma, with MSWD = 0.92 (Figure 5c,d).

The Th content of TS19085–2 zircon ranged between 58.20 ppm and 401.75 ppm, while the U content ranged between 58.82 ppm and 589.59 ppm. The Th/U ratio ranged between 0.41 and 1.11 and a majority of the Th/U ratios exceeded 0.4. The positive correlation between Th and U indicates the magmatic origin of zircon. The distribution pattern of REEs demonstrates a left-leaning curve of HREE type, indicating negative Eu and positive Ce anomalies (Figure 4c) (Supplementary Table S1). U-Pb isotope age analysis was performed on 25 zircons sampled from Banpo pluton and 25 points were determined (Supplementary Table S2). Among these, 19 zircons demonstrated good concordant values of  $^{206}\text{Pb}/^{238}\text{U}$ , and the remaining  $^{206}\text{Pb}/^{238}\text{U}$  age values ranged between 203 Ma and 224 Ma. A majority of the zircon data points aligned with the concordant diagram are at or near the concordant line. The weighted average age value of  $^{206}\text{Pb}/^{238}\text{U}$  corresponds to  $216.3 \pm 2.3$  Ma, with MSWD = 1.6 (Figure 5e,f). All three age values were within the acceptable error limit. Therefore, the crystallization ages of Banpo pluton were  $213.4 \pm 2.1$  Ma,  $213.0 \pm 1.6$  Ma, and  $216.3 \pm 2.3$  Ma, indicating the occurrence of the rock formation in the Late Triassic Norian.

## 5.2. Major and Trace Element Geochemistry

### 5.2.1. Major Elements

The  $\text{SiO}_2$  content of three samples ranges from 55.21% to 58.43%, while the content of the remaining samples ranges from 68.41% to 74.92%, with an overall average of 68.42%, indicating a high  $\text{SiO}_2$  content. In the TAS diagram (Figure 6a), the vast majority of samples are located within the granite region, while three samples are located within the coarse-grained andesite region. The  $\text{K}_2\text{O}$  content ranges from 5.11% to 6.53%, the  $\text{Na}_2\text{O}$  content ranges from 2.83% to 4.20%, and the  $\text{Na}_2\text{O} + \text{K}_2\text{O}$  content ranges from 7.53% to 10.73%, with an average value of 9.41%. It belongs to the calcium alkaline series. The alkalinity (AR) ranges from 2.11 to 4.81, with a relatively high alkali content. The  $\text{K}_2\text{O}/\text{Na}_2\text{O}$  ratio ranges from 1.30 to 2.24, indicating potassium-rich characteristics.

The alkaline index (AI) varied from 0.60–0.88, indicating higher alkalinity. In the  $\text{SiO}_2$ - $\text{K}_2\text{O}$  diagram (Figure 6b), a majority of the samples are located within the potassium region, with only 2 samples within the high potassium and calcium alkaline region. In the  $\text{SiO}_2$ -( $\text{Na}_2\text{O} + \text{K}_2\text{O}$ - $\text{CaO}$ ) diagram (Figure 6c), the samples are located within the alkaline region. The  $\text{Al}_2\text{O}_3$  content varied from 13.44% to 17.58%, with an average of 15.42%. The aluminum saturation index, i.e., the A/CNK value, is between 0.88 and 1.09, indicating a weakly peraluminous rock. In the A/NK-A/CNK diagram (Figure 6d), the samples are located within the peraluminous region, while Banpo pluton is primarily located within the peraluminous area.

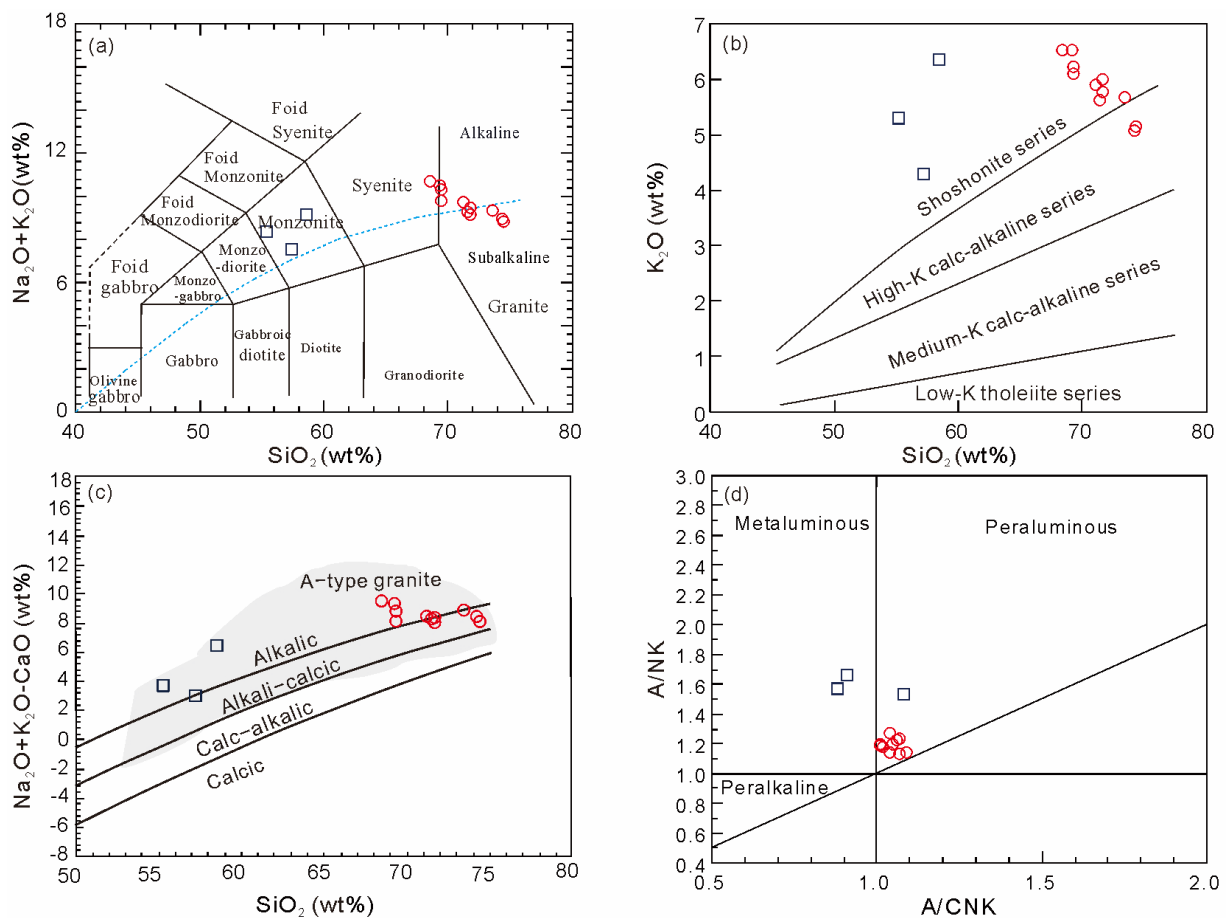


**Figure 6.** (a) TAS diagrams (after Middlemost [59]); (b)  $\text{K}_2\text{O}$  vs  $\text{SiO}_2$  diagrams (after Rickwood [60]); (c)  $(\text{Na}_2\text{O} + \text{K}_2\text{O} - \text{CaO}) - \text{SiO}_2$  diagrams (after Frost et al. [61]); and (d) A/NK–A/CNK diagrams (after Maniar et al. [62]) for the Banpo pluton in WNQOB.

### 5.2.2. Trace Elements

A significantly high REEs content of the Banpo pluton was observed, with an  $\Sigma\text{REE}$  ranging from 142.89 ppm to 411.44 ppm and averaging 337.07 ppm (Supplementary Table S3). The region was strongly enriched with light rare earth elements (LREE), with  $\Sigma\text{LREE}$  ranging from 124.68 ppm to 390.40 ppm and averaging 316.37 ppm. As a result, the region was characterized by a significant loss of HREE, with  $\Sigma\text{HREE}$  ranging from 17.21 ppm to 26.31 ppm and averaging 20.70 ppm. The LREE/HREE ratio was 6.85–19.69. The  $(\text{La}/\text{Yb})_N$  ratio ranged from 7.47 to 29.83. Similarly,  $\delta\text{Eu}$  ranged from 0.15 to 0.77, exhibiting a strong negative Eu anomaly. Chondrite-normalized REE patterns (Figure 7a) demonstrate a right dipping type with strong LREE enrichment, indicating the possible occurrence of garnet, rutile.

The spider diagram of primitive mantle-normalized trace elements shows enrichment in large ion lithophile elements such as Rb and La, as well as the presence of high field strength elements like Zr, Hf, and Pb (Figure 7b). Conversely, certain elements such as Ba, Sr, Nb, Ta, etc., exhibit relative depletion.

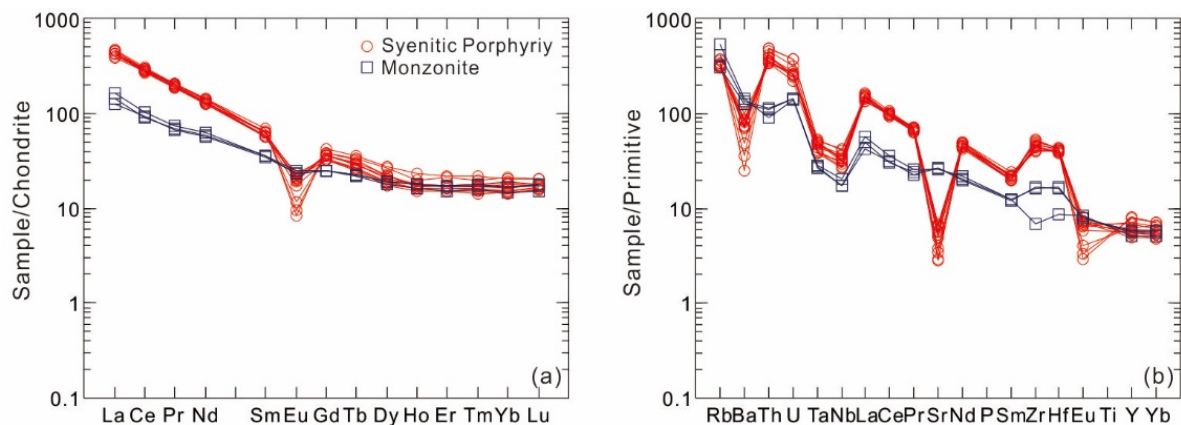


**Figure 7.** (a) Chondrite-normalized rare earth element (REE) patterns; and (b) primitive-normalized incompatible element distribution patterns for the Banpo pluton in WNQOB (chondrite data and primitive data for normalization taken from Sun and McDonough [63]).

## 6. Discussion

### 6.1. Magma Source

Syenite is a type of alkaline rock representing post-collision, intraplate extension, or rift tectonic settings [38,40,41,64,65]. It can provide certain important information, such as the evolutionary relationship between continental lithosphere crust and mantle in the post-collision or intraplate tension settings. There are several perspectives on the origin of syenite-like rocks. Some researchers suggest that they are formed by a low degree of partial melting of heterogeneous lower crustal materials involving volatile matter or under high-pressure conditions [66,67]. Other researchers propose partial melting of the enriched lithospheric mantle, which is a product of the crystallization differentiation of alkaline basaltic magma [68–70] and their formation by magma mixing, primarily because the mantle-derived mafic magma and crust-derived felsic magma undergo mixing to induce melting and further differentiation. Alternatively, they may be formed by the mixing of alkaline magma with mantle-derived silica unsaturated and crustal-derived granitic magma [71–73]. Presently, several researchers believe that the formation of Syenite-like rocks is mainly attributable to mantle source components [74,75].

The experimental petrology results also confirmed that syenite magma is related to mantle or mantle-derived materials. Based on the melting of experimental data from synthetic granite systems, i.e., the decrease in quartz content in the melt and the increase in albite content with the increase in pressure, Huang and Wyllie [65] speculated that the melting of continental crust rocks at the bottom of the thickened continental crust forms trachyte (syenite) rather than granitic magma. Further, Deng J. F. et al. [76] provided additional evidence to support this hypothesis from the perspective of rock phase equilibrium, referred to as high-pressure syenite, formed by partial melting of the crust with a pressure greater than 1.5 GPa and inferred that it exhibits a rare earth distribution pattern without negative europium anomaly. Low-pressure ( $P < 1.5$  Gpa) syenite is derived from the separation of plagioclase from basaltic magma and has evident negative europium anomaly [77]. However, the experiment by Litvinovsky et al. [78] demonstrated that the partial melting of felsic rocks under the condition of thickened crust does not produce syenitic magma; instead, it results in granitic magma. Similarly, the melting experiments conducted by metasomatic mantle rocks demonstrated the production of silica-unsaturated nephelinite and other peralkaline rocks under high pressure. On the other hand, under low pressure, low melting can produce silica-saturated trachyandesite and other potassic magma and serve as the parent magma of potassic syenite [79]. Long X. P. et al. [80] also obtained highly alkaline syenite (trachytic) melts through water loss melting of potassium-rich basaltic rocks (basaltic rocks) under high pressure. The petrology characteristics of the above rock experiments demonstrated that the melting of potassium-rich basic rocks or rich mantle

rocks at the bottom of the thickened crust could form potassium-rich alkali syenitic magma or its parent magma. Conversely, the felsic rocks in the thickened continental crust cannot form syenitic magma and, as a result, the negative europium anomaly is not significant. Similarly, silica-saturated Syenite formed by the melting in a low-pressure environment is derived from magma produced after the separation of plagioclase from basaltic magma, with significant negative europium anomaly.

### 6.2. Tectonic Setting

The genesis of Banpo pluton can be related to the late collision strike–slip environment after the collision between the North China Block and the Yangtze Block [8,81–84]. It was observed that a series of derived strike–slip pull-apart basins are often developed along the strike–slip faults. In system, several potassic alkali-rich igneous rocks also appeared, which are considered to be controlled by the intracontinental strike–slip transformation tectonic stress field [4,47,85]. The REE of Banpo pluton exhibits a significant negative europium anomaly which is inconsistent with the experimental results of felsic matter melting to form syenite magma under controlled conditions. The rock mass also had a high SiO<sub>2</sub> content, with an average value of 68.42%, indicating that the silica content had reached saturation. Thus, it can be inferred that the rock mass is unlikely to be a product of the partial melting of crustal material under crustal thickening conditions. Instead, it is a syenite magma formed by the melting in an extensional decompression environment, which is contaminated by crustal materials during ascending emplacement, leading to magma mixing with them. In addition, it is observed that the Banpo pluton contains a certain amount of mafic enclave inclusions, revealing that the Banpo pluton intrusion is a product of mixing and further differentiation of syenite parental magma formed through the low melting of mantle-derived mafic magma at reduced pressure and crust-derived materials.

The unipolar photomicrographs of the Banpo pluton frequently demonstrated a banded structure of potassium feldspar surrounding quartz, indicating a large temperature difference in its formation. As a result of the mixing and solidification of magma, a potassium feldspar banded structure is formed surrounding the high-temperature quartz. Alkaline granite (A<sub>1</sub>) in anorogenic environments within the plate exhibits a high Nb/Ta ratio (15.7–17.5) due to the addition of more mantle-derived or enriched mantle materials within the source area. The alkaline granite formed in post-collision environments (A<sub>2</sub> type, with a large amount of lower crust within the source area) exhibits a low Nb/Ta ratio, generally around 10–14 [85]. The Nb/Ta ratio of Banpo pluton varies from 11.20 to 14.49, with an average of 12.54. This shows a significant deviation from the Nb/Ta ratio of the original mantle, while the overall ratio is in agreement with that of the continental crust (Nb/Ta = 10 to 14 [86]), indicating the contamination of magma of Banpo pluton with the crustal materials during its ascent. The initial syenitic parent magma formed through the low partial melting of mantle-derived mafic magma at reduced pressure serves as a heat source for the melting of lower crustal materials and undergoes mixing with them to a certain extent. Subsequently, it further crystallizes and differentiates to form Banpo pluton.

Numerous syenite types found globally are generally associated with A-type granite, indicating a certain relationship and common geochemical characteristics between the two in terms of genesis [87]. Therefore, several scholars classified syenite as A-type granite. The high rare earth abundance, a seagull-type right dip partitioning curve, high alkali content, potassium-rich composition, and weakly peraluminous characteristics of the western Banpo pluton in the North Qinling Orogenic Belt are in agreement with the typical characteristics of A-type granite [35]. In the rock type discrimination diagram (Figure 8), all the rocks studied are classified within the A-type granite region. The zircon saturation temperature calculations for Banpo pluton also indicated its formation at higher temperatures (temperatures ranging from 706–907 °C, with an average temperature of 860 °C), which is consistent with the formation temperature of A-type granite higher than the formation temperatures of I-type and S-type granites. The average temperature of S-type granite is 764 °C, while that of I-type granite is 781 °C [41]. In addition, its output

strike-slip extensional environment aligns with the stress environment consistent with the extension of A-type granite output.

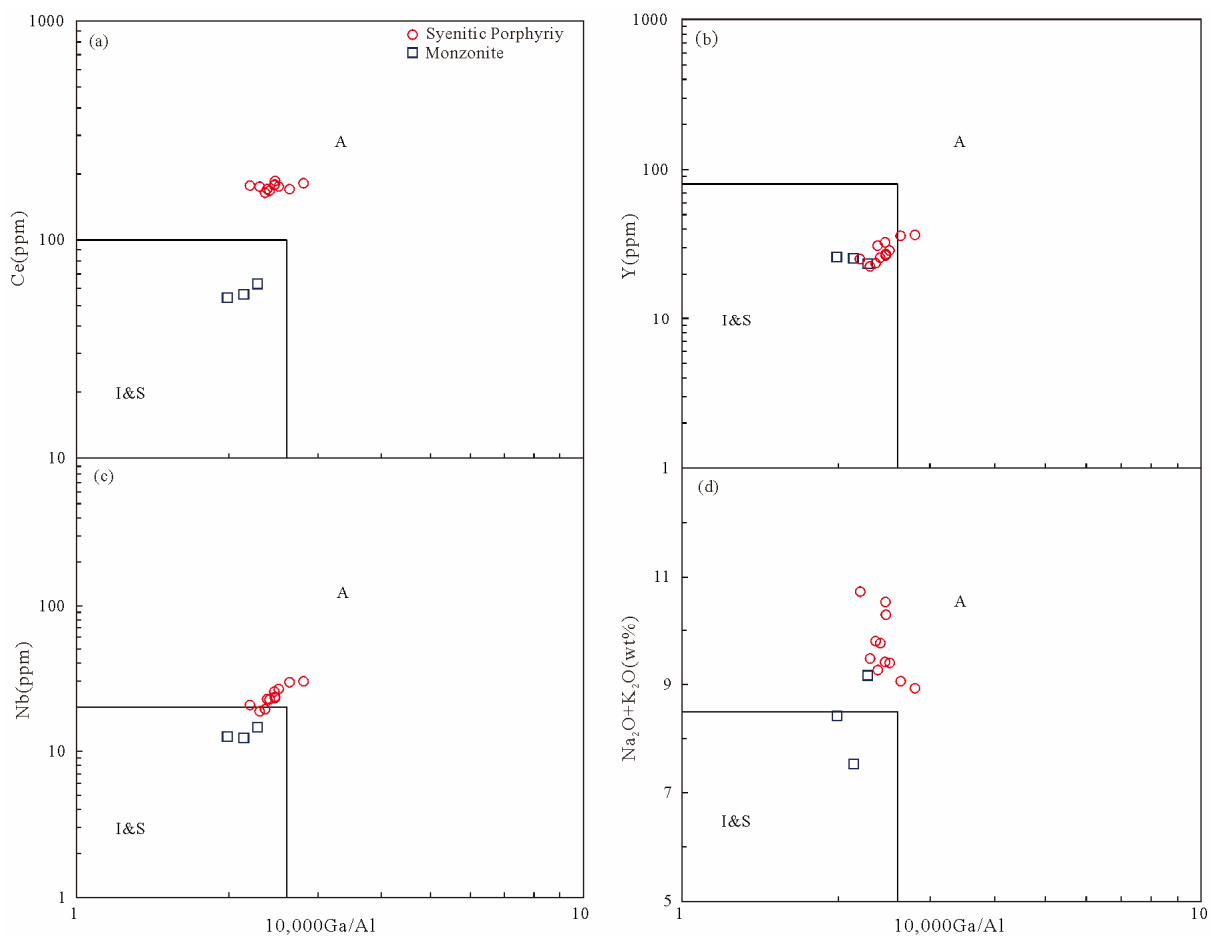


**Figure 8.** (a)  $(\text{Na}_2\text{O} + \text{K}_2\text{O})$ , (b) Nb, (c)  $\text{MgO}/\text{K}_2\text{O}$ , and (d)  $(\text{K}_2\text{O} + \text{Na}_2\text{O})/\text{CaO}$  vs.  $10,000 \text{ Ga}/\text{Al}$  discrimination diagrams for the Banpo pluton in the WQOB (after Whalen et al. [38]). A = A-type granitoids; I = I-type granitoids; and S = S-type granitoids.

During the Mesozoic, the most prominent feature at the Qinling–Qilian junction was the development of numerous 245–205 Ma-dominated granites of various types. There are diverse interpretations regarding the formation and tectonic background of these granites, such as synorogenic granite [88], post-collision granite [7,8,89], and anorogenic granite [90]. The statistical results of granite body formation ages indicated further differentiation into the early Indosinian period (243–233 Ma) and the late Indosinian period (220–205 Ma) [91]. The early Indo granites are generally characterized by the geochemical characteristics of island arc and formed by the partial melting of the thickened lower crust formed through continental subduction or continental collision [48]. On the other hand, late Indosinian granites generally show the characteristics of post-collisional granites [21,92,93]. All the samples of Banpo pluton are located near collisional and intraplate granites on the tectonic environment discrimination map (Figure 9a,b), indicating the intrusion formed in the post-collisional extension environment.

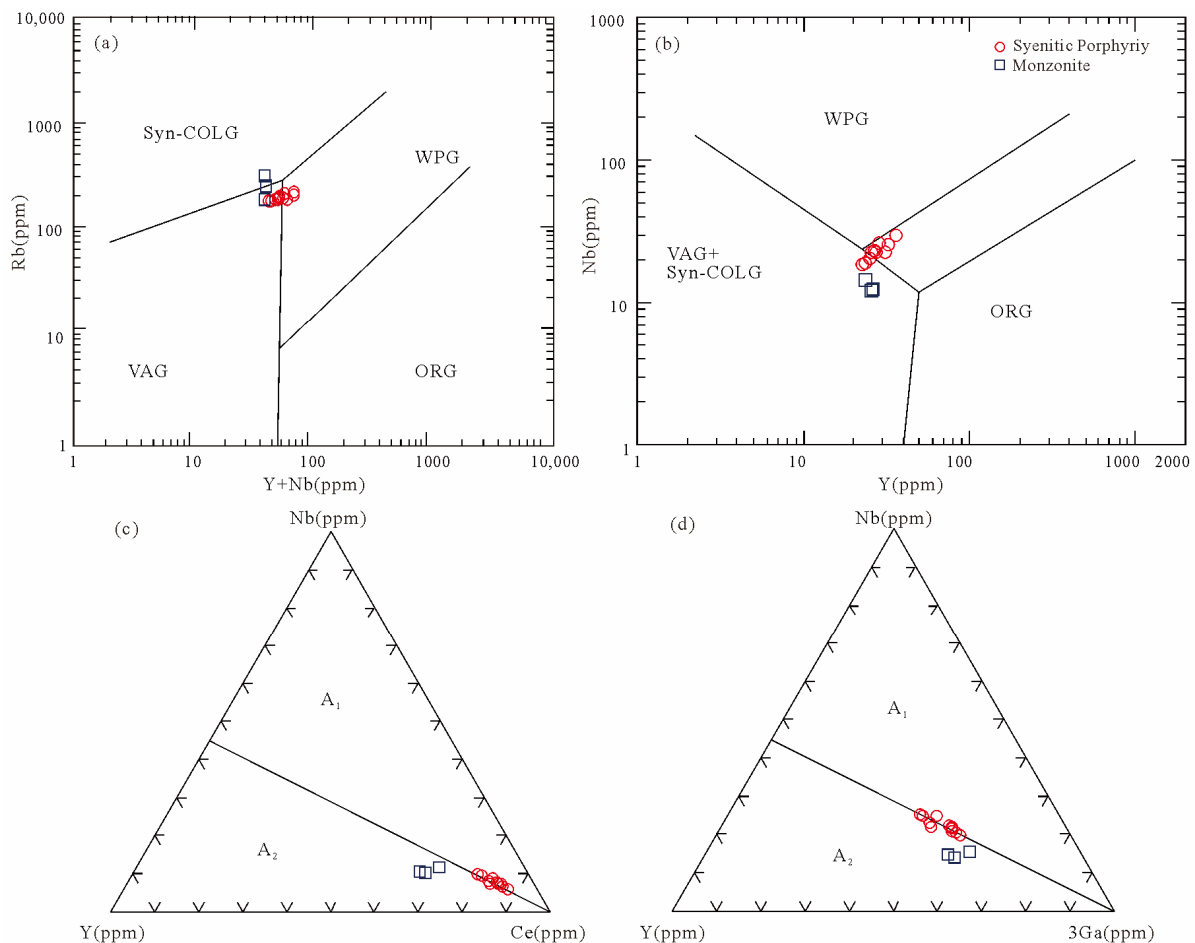


**Figure 9.** (a) Nb–Y diagrams; (b) Ta–Yb diagrams for the Banpo pluton the WNQOB (after Pearce et al. [94]); (c) Nb–Y–3Ga diagrams; and (d) Nb–Y–Ce diagrams for the S Banpo pluton the WNQOB (after Eby [40]). VAG = volcanic arc granites; Syn-COLG = syn-collision granites; WPG = within-plate granites; ORG = ocean ridge granites; A1-type = anorogenic environment; and A2-type = post-Orogenic environment.

On the classification diagram of A-type granite subclasses Nb–Ce–Y and Nb–3Ga–Y (Figure 9c,d), all samples are positioned near the boundary between A<sub>1</sub>-type granite and A<sub>2</sub>-type granite, leaning toward the A<sub>2</sub>-type granite side. This suggests that they were formed during the transitional stage from post-Orogenic to non-Orogenic environments. The researchers believe that A-type granite is formed in an extensional environment [87,95–98]. Considering the petrogenesis and regional characteristics, we believe that the Banpo pluton formed in the post-Orogenic extensional environment after the subduction of the South China Block towards the North China Block.

### 6.3. Geological Significance

Numerous studies have shown that during the Indosinian period, a collision orogeny took place in the central Orogenic system of North China, Qinling, and Yangtze Blocks. This resulted in the Qinling Orogenic Belt transitioned into a typical intracontinental collisional orogeny as the Yangtze Block subducting beneath the Qinling micro-block along the Mianxian–Lueyang suture zone. This led to crustal thickening [28,99–104]. The thickened crust experienced significant heating and pressure, leading to widespread melting and the development of various intermediate-acid intrusive rocks in the Qinling Orogenic Belt (from west of the Henan Shaanxi border to the Tianshui area). The increased internal temperature of the crust caused partial melting of different types of rocks, resulting in the formation of diverse types of granitic magma. Experimental petrology research indicates

that at depths below 20 km under the crust, when the temperature reaches around 900 °C and water is present, intrusive magma with strong upwelling capacity can be generated, either forming hypabyssal or ultra-hypabyssal granite bodies or erupting to the surface as rhyolite [77,105]. Achieving such high temperatures of around 900 °C and partial melting in the thickened lower crust during collision orogeny is challenging unless there is an external heat supply from other sources [105]. The saturation temperature of zirconium in the Banpo pluton was calculated to obtain the magma crystallization temperature (ranging from 706 °C to 907 °C, with an average temperature of 860 °C). Such high temperatures are more likely to originate from mantle sources [106]. After the completion of the collision orogeny in the Indosinian period, the North China Block and the Yangtze Block entered the lithosphere stretching stage, with mafic magma derived from the mantle intruding into the lower crust [107,108]. This mafic magma provided heat for partial melting in the source area and contributed a small amount of mantle-derived material to the newly released magma. This indicates that the eastern part of the North Qinling Orogenic Belt completed the primary collision orogeny during the late Indosinian period. Subsequently, the region underwent relaxation and gravity adjustments during the late Orogenic period, transitioning into an extensional rifting phase in the post-Orogenic stage. This phase is characterized by the formation of intermountain fault basins and pull-apart basins caused by block faulting, shear translation, and the occurrence of corresponding potassic alkali-rich igneous rocks.

## 7. Conclusions

(1) The LA-ICP-MS zircon U-Pb dating results indicate that the Banpo pluton in the western section of the North Qinling Orogenic Belt was formed during the Late Triassic Norian, with ages of 213.4 Ma  $\pm$  2.1 Ma (MSWD = 0.56), 213.0 Ma  $\pm$  1.6 Ma (MSWD = 0.92), and 213.2 Ma  $\pm$  4.4 Ma (MSWD = 1.6).

(2) The Banpo pluton in this region displays several characteristics, such as high rare earth abundance, a seagull-type right-dip partitioning curve, high alkali, and potassium content, and weakly peraluminous composition. These features are consistent with A<sub>2</sub>-type granite, suggesting that it was formed during the transitional stage from post-Orogenic to non-Orogenic environments.

(3) In the late Late Triassic period, the western section of the North Qinling Orogenic Belt was a post-Orogenic extensional environment and A<sub>2</sub>-type granites were formed.

**Supplementary Materials:** The following supporting information can be downloaded at: <https://www.mdpi.com/article/10.3390/min14030222/s1>, Table S1: Zircon trace element data of the Late Triassic orthophyre in the western part of the NQOB; Table S2: Zircon LA-ICP-MS U-Pb data of the Late Triassic orthophyre in the western part of the NQOB; and Table S3: Whole-rock major and trace element data of the Late Triassic orthophyre in the western part of the NQOB.

**Author Contributions:** Conceptualization, S.L. and Z.L.; methodology, S.L. and X.P.; software, H.L., L.Q., S.J. and Y.Y.; validation, S.L., Z.L. and S.J.; formal analysis, S.L., Z.L. and H.L.; investigation, S.L., Z.L., X.P., H.L., L.Q., H.L., S.J. and J.R.; resources, S.L. and Z.L.; data curation, S.L. and Z.L.; writing—original draft preparation, S.L. and Z.L.; writing—review and editing, S.L., Z.L. and H.L.; visualization, S.L.; supervision, S.L. and Z.L.; project administration, Z.L.; funding acquisition, Z.L. All authors have read and agreed to the published version of the manuscript.

**Funding:** This research was funded by the National Nature Sciences Foundation of China (grant nos. 41872235, 42172236, 41872234, and 41502191), the Natural Science Basic Research Plan in Shaanxi Province of China (grant nos. 2019JM-312, 2019JQ-090, 2019JQ-209, and 2020JM-229), the Fundamental Research Funds for the Central Universities (grant nos. 300102270202, 300103183081, 300103120009, 300104282717, 300102279204, and 201810710233), the China Scholarship Council (grant no. 201806565026), and the Youth Innovation Team of Shaanxi Universities.

**Data Availability Statement:** The original contributions presented in the study are included in the article/Supplementary Materials.

**Acknowledgments:** Our thanks are extended to the chief editor and the two anonymous reviewers for their constructive reviews which have greatly improved our manuscript.

**Conflicts of Interest:** The authors declare no conflicts of interest.

## References

- Zhang, G.W.; Meng, Q.R.; Lai, S.C. Structures and Tectonics of the QinLing Orogenic belt. *Sci. China* **1995**, *25*, 994–1003. (In Chinese)
- Li, S.G.; Sun, W.D.; Zhang, G.W.; Chen, J.Y.; Yang, Y.C. Chronology and Geochemistry of HeiGouxia Metamorphic Volcanic Rocks in Mian-Lue Tectonic Belt, South Qinling: Evidence of the Paleozoic Ocean Basin and Its Closure age. *Sci. China* **1996**, *03*, 223–230. (In Chinese)
- Feng, Y.M.; Cao, X.D.; Zhang, E.P. Tectonic Evolution Framework and Nature of the West Qinling Orogenic Belt. *Northwest. Geol.* **2003**, *36*, 1–10. (In Chinese with English abstract)
- Pei, X.Z.; Ding, S.P.; Hu, B. Geochemical characteristics and tectonic significance of Cenozoic acid volcanic rocks in Tianshui area, West Qinling Mountains. *Acta Mineral. Sin.* **2004**, *23*, 227–235. (In Chinese with English abstract)
- Dong, Y.P.; Zhang, X.N.; Liu, X.M.; Li, W.; Chen, Q.; Zhang, G.W.; Zhang, H.F.; Zhao, Y.; Sun, S.S.; Zhang, F.F. Propagation tectonics and multiple accretionary processes of the Qinling Orogen. *J. Asian Earth Sci.* **2015**, *104*, 84–98. [[CrossRef](#)]
- Dong, Y.P.; Sun, S.S.; Santosh, M.; Hui, B.; Sun, J.P.; Zhang, F.F.; Cheng, B.; Yang, Z.; Shi, X.H.; He, D.F.; et al. Cross Orogenic Belts in Central China: Implications for the tectonic and paleo geographic evolution of the East Asian continental collage. *Gondwana Res.* **2022**, *109*, 18–88. [[CrossRef](#)]
- Zhang, H.F.; Jin, L.L.; Zhang, L.; Yuan, H.-L.; Zhou, L.; Zhang, B.-R. Pb and Nd Isotopic Compositions of Basement and Granitoid in the Qilianshan: Constraints on Tectonic Affinity. *Earth Sci.* **2006**, *1*, 57–65. (In Chinese with English abstract)
- Luo, B.J.; Zhang, H.F.; Xiao, Z.Q. Petrogenesis and tectonic implications of the Early Indosinian Meiwu Pluton in WestQinling, central China. *Earth Sci. Front.* **2012**, *19*, 199–213. (In Chinese with English abstract)
- Wang, X.X.; Wang, T.; Zhang, C.L. Neoproterozoic, Paleozoic, and Mesozoic granitoid magmatism in the Qinling Orogen, China: Constraints on orogenic process. *J. Asian Earth Sci.* **2013**, *72*, 129–151. [[CrossRef](#)]
- Huang, X.F.; Mo, X.X.; Yu, X.H.; Li, X.W.; Yang, M.C.; Luo, M.F.; He, W.Y.; Yu, J.C. Origin and geodynamic settings of the Indosinian high Sr/Y granitoids in the West Qinling: An example from the Shehalijipluton in Tongren area. *Acta Petrol. Sin.* **2014**, *30*, 3255–3270. (In Chinese with English abstract)
- Zhang, G.W.; Guo, A.L.; Yao, A.P. Qilian East Songpan Continental Tectonic Knot in Chinese Mainland. *Earth Sci. Front.* **2004**, *3*, 23–32. (In Chinese with English abstract)
- Zhao, D.H.; Ping, X.Q.; Zheng, J.P.; Ai, L.; Deng, H. Geochemistry and Its Geological Significance of the Quartz Syenites in the Early Indosinian from the Tietang Gorge, West Qinling. *Earth Sci.* **2019**, *44*, 4203–4221. (In Chinese with English abstract)
- Pei, X.Z.; Zhang, G.W.; Lai, S.C.; Li, Y.; Chen, L.; Gao, M. Main geological features of the Mianlue tectonic belt on the southern margin of the West Qinling. *Geol. Bull. China* **2002**, *21*, 486–494. (In Chinese with English abstract)
- Dong, Y.P.; Zhang, G.W.; Neubauer, F.; Liu, X.M.; Genser, J.; Hauzenberger, C. Tectonic evolution of the Qinling orogen, China: Review and synthesis. *J. Asian Earth Sci.* **2011**, *41*, 213–237. [[CrossRef](#)]
- Dong, Y.P.; Sun, S.S.; Santosh, M.; Zhao, J.; Sun, J.P.; He, D.F.; Shi, X.H.; Hui, B.; Cheng, C.; Zhang, G.W. Central China Orogenic Belt and amalgamation of East Asian continents. *Gondwana Res.* **2021**, *100*, 131–194. [[CrossRef](#)]
- Pan, G.T. Tethyan evolution in global ocean land transition. *Tethyan Geol.* **1994**, *18*, 23–40. (In Chinese with English abstract)
- Xu, Z.Q.; Yang, J.S.; Li, W.C.; Li, H.Q.; Cai, Z.H.; Yan, Z.; Ma, C.Q. Paleo-Tethys system and accretionary orogen in the Tibet Plateau. *Acta Petrol. Sin.* **2013**, *29*, 1847–1860.
- Xu, X.Y.; Chen, J.L.; Yan, Z.; Wang, R.T.; Li, P.; Li, T.; Wang, H.L.; Yang, Y.Z.; Yang, J.L.; Li, Z.P.; et al. *Geological Map (1:500,000) of Qinling and Adjacent Areas*; Xi'an Map Publishing House: Xi'an, China, 2014. (In Chinese with English abstract)
- Huang, X.F.; Mo, X.X.; Yu, X.H.; Li, X.W.; Ding, Y.; Wei, P.; Wen, Y. Zircon U-Pb chronology, geochemistry of the Late Triassic acid volcanic rocks in Tanchang area, West Qinling and their geological significance. *Acta Petrol. Sin.* **2013**, *29*, 3968–3980. (In Chinese with English abstract)
- Xu, X.Y.; Wang, H.L.; Chen, J.L.; Su, X.H.; Wu, P.; Gao, T. Zircon U-Pb age, element geochemistry of Mesozoic acid volcanic rocks at Yindaoshi area in western Qinling. *Acta Petrol. Sin.* **2007**, *23*, 2845–2856. (In Chinese with English abstract)
- Xu, X.Y.; Chen, J.L.; Gao, T.; Li, P.; Li, T. Granitoid magmatism and tectonic evolution in northern edge of the Western Qinling terrane, NW China. *Acta Petrol. Sin.* **2014**, *30*, 371–389. (In Chinese with English abstract)
- Wang, X.X.; Wang, T.; Zhang, C.L. Granitoid magmatism in the Qinling orogen, central China and its bearing on orogenic evolution. *Sci. China Earth Sci.* **2015**, *58*, 1497–1512. (In Chinese) [[CrossRef](#)]
- Li, X.W.; Mo, X.X.; Huang, X.F.; Dong, G.C.; Yu, X.H.; Luo, M.F.; Liu, Y.B. U-Pb zircon geochronology, geochemical and Sr-Nd-Hf isotopic compositions of the Early Indosinian Tongren pluton in West Qinling: Petrogenesis and geodynamic implications. *J. Asian Earth Sci.* **2015**, *97*, 38–50. [[CrossRef](#)]
- Qiu, K.F.; Yu, H.C.; Gou, Z.Y.; Liang, Z.L.; Zhang, J.L.; Zhu, R. Nature and origin of Triassic igneous activity in the Western Qinling Orogen: The Wenquan composite pluton example. *Int. Geol. Rev.* **2018**, *60*, 242–266. [[CrossRef](#)]

25. Xiong, X.; Zhu, L.M.; Zhang, G.W.; Santosh, M.; Jiang, H.; Zheng, J.; Guo, A.L.; Ding, L.L. Petrogenesis and tectonic implications of Indosinian granitoids from Western Qinling Orogen, China: Products of magma-mixing and fractionation. *Geosci. Front.* **2020**, *11*, 1305–1321. [[CrossRef](#)]
26. Xing, H.Q.; Li, X.W.; Xu, J.F.; Mo, X.X.; Shan, W.; Yu, H.X.; Hu, J.Q.; Huang, X.F.; Dong, G.C. The genesis of felsic magmatism during the closure of the northeastern Paleo-Tethys Ocean: Evidence from the Heri batholith in West Qinling, China. *Gondwana Res.* **2020**, *84*, 38–51. [[CrossRef](#)]
27. Yin, A.; Nie, S.Y. An indentation model for the North and South China collision and the development of the Tan-Lu and Honam fault systems, eastern Asia. *Tectonics* **1993**, *12*, 801–813. [[CrossRef](#)]
28. Lu, X.X.; Dong, Y.; Chang, Q.L.; Xiao, Q.H.; Li, X.B.; Wang, X.X. Qinling Indosinian Shahewan Ordovician rapakivi granite and its dynamic significance. *China* **1996**, *03*, 244–248. (In Chinese)
29. Zhang, B.R. Tectonic-Geochemistry district and orogenic movement model in Qinling Mountains. National key laboratory for metallogenic studies, department of earth sciences, nanjing university. Paper summary set of the 4th world symposium on Chinese geological sciences. In Proceedings of the 4th World Chinese Geological Science Symposium, Nanjing, China, 22–23 May 2002; Volume 4, pp. 274–277. (In Chinese with English abstract)
30. Wang, X.X.; Wang, T.; Jahn, B.-M.; Hu, N.G.; Chen, W. Tectonic significance of Late Triassic post-collisional lamprophyre dykes from the Qinling Mountains (China). *Geol. Mag.* **2007**, *144*, 837–848. [[CrossRef](#)]
31. Chen, Y.J.; Santosh, M. Triassic tectonics and mineral systems in the Qinling Orogen, central China. *Geol. J.* **2014**, *49*, 338–358. [[CrossRef](#)]
32. Li, X.F.; Li, Y.S.; Dong, G.C.; Li, X.; Xia, Q. Granitoid magmatism and tectonic evolution in the eastern part of the West Qinling; Constraints from geochemistry, zircon U-Pb chronology and Hf isotopic. *Acta Petrol. Sin.* **2021**, *37*, 1691–1712. (In Chinese with English abstract)
33. Qian, Z.S.; Yang, F.; Chao, L.; Xue, F.; Santosh, M.; Yang, B.; Zhang, S.; Kim, S.W. Late Mesozoic Huang beiling S-type granite in the East Qinling Orogen, China: Geochronology, petrogenesis and implications for tectonic evolution. *Geochemistry* **2022**, *82*, 125857. [[CrossRef](#)]
34. Li, X.; Dong, G.; Yu, X.; Li, Y.; Santosh, M.; Lv, X.; Xia, Q. Evidence for magma mixing during triassic magmatism in west Qinling, china: Constraints from petrology, geochemistry, U-Pb zircon geochronology, and Sr-Nd-Hf isotopic of the baguashan pluton. *Geol. J.* **2021**, *56*, 5255–5274. [[CrossRef](#)]
35. Bai, B.W.; Chen, D.L.; Zhu, X.H.; Ren, Y.F.; Luo, F.H.; Wang, H.J. A-type granite and dark enclaves in the North Qinling Orogenic Belt: Constrains on the tectonic affinity between the North Qinling Orogenic Belt and the North China Craton. *Precambrian Res.* **2021**, *357*, 106–117. [[CrossRef](#)]
36. Ma, J.; Lü, X.B.; Li, S.; Chen, J.J.; Lu, F.; Yin, X.; Wu, M.Q. The ca. 230 ma gold mineralization in the fengtai basin, western Qinling orogen, and its implications for ore genesis and geodynamic setting: A case study of the matigou gold deposit. *Ore Geol. Rev.* **2021**, *138*, 104398. [[CrossRef](#)]
37. Loiselle, M.C.; Wones, D.R. Characteristics and origin of anorogenic granites. *Geol. Soc. Am. Abstr. Prog.* **1979**, *11*, 468.
38. Collins, W.J.; Beams, S.; White, A.J.R.; Chappell, B.W. Nature and origin of A-type granites with particular reference to southeastern Australia. *Contrib. Mineral. Petrol.* **1982**, *80*, 189–200. [[CrossRef](#)]
39. Whalen, J.B.; Currie, K.L.; Chappell, B.W. A-type granites: Geochemical characteristics, discrimination and petrogenesis. *Contrib. Mineral. Petrol.* **1987**, *95*, 407–419. [[CrossRef](#)]
40. Eby, G.N. The A-type granitoids: A review of their occurrence and chemical characteristics and speculations on their petrogenesis. *Lithos* **1990**, *26*, 115–134. [[CrossRef](#)]
41. Eby, G.N. Chemical subdivision of the A-type granitoids: Petrogenetic and tectonic implications. *Geology* **1992**, *20*, 641–644. [[CrossRef](#)]
42. Bonin, B. From orogenic to anorogenic settings: Evolution of granitoid suites after a major orogenesis. *Geol. J.* **1990**, *25*, 261–270. [[CrossRef](#)]
43. Bonin, B. A-type granites and related rocks: Evolution of a concept, problems and prospects. *Lithos* **2007**, *97*, 1–29. [[CrossRef](#)]
44. King, P.L.; White, A.J.R.; Chappell, B.W.; Allen, C.M. Characterization and Origin of Aluminous A-type Granites from the Lachlan Fold Belt, Southeastern Australia. *J. Petrol.* **1997**, *38*, 371–391. [[CrossRef](#)]
45. Mushkin, O.; Navon, L.; Halicz, L.; Hartmann, G.; Stein, M. The Petrogenesis of A-type Magmas from the Amram Massif, Southern Israel. *J. Petrol.* **2003**, *44*, 815–832. [[CrossRef](#)]
46. Xiao, E.; Qiu, J.S.; Xu, X.S.; Jiang, S.Y.; Hu, J.; Li, Z. Chronology, geochemistry, petrogenesis and tectonic implications of Yaokeng Alkaline granites in Zhejiang Province. *Acta Petrol. Sin.* **2007**, *23*, 1431–1440. (In Chinese with English abstract)
47. Abuduxun, N.; Windley, B.F.; Xiao, W.; Zhang, J.E.; Chen, Y.C.; Huang, P.; Gan, J.M.; Sang, M. Carboniferous tectonic incorporation of a Devonian seamount and oceanic crust into the South Tianshan accretionary orogen in the southern Altaids. *Int. J. Earth Sci.* **2021**, *111*, 2535–2553. [[CrossRef](#)]
48. Zhang, G.W.; Dong, Y.P.; Yao, A.P. Review on the development of studies on the tectonic and orogen process of orogenic belt, and discussing on some new key problems. *Northwest. Geol.* **2001**, *34*, 1–9. (In Chinese with English abstract)
49. Gao, S.; Liu, X.M.; Yuan, H.L.; Hattendorf, B.; Günther, D.; Chen, L.; Hu, S.H. Analysis of forty-two major and trace elements of USGS and NIST SRM glasses by LA-ICP-MS. *Geostand. Newsl.* **2002**, *26*, 181–196. [[CrossRef](#)]

50. Liu, Y.; Gao, S.; Hu, Z.; Gao, C.; Zong, K.; Wang, D. Continental and oceanic crust recycling-induced melt-peridotite interactions in the Trans-North China Orogen: U-Pb dating, Hf isotopes and trace elements in zircons from mantle xenoliths. *J. Petrol.* **2010**, *51*, 537–571. [[CrossRef](#)]
51. Liu, Y.S.; Hu, Z.C.; Gao, S.; Ginther, D.; Xu, J.; Gao, C.G.; Chen, H.H. In situ analysis of major and trace elements of anhydrous minerals by LA-ICP-MS without applying an internal standard. *Chem. Geol.* **2008**, *257*, 34–43. [[CrossRef](#)]
52. Andersen, T. Correction of common lead in U-Pb analyses that do not report <sup>204</sup>Pb. *Chem. Geol.* **2002**, *192*, 59–79. [[CrossRef](#)]
53. Ludwig, K.R. *Using Isoplot/EX, Version 2.49: A Geochronological Toolkit for Microsoft Excel*; Berkeley Geochronological Center Special Publication: Berkeley, CA, USA, 2001; pp. 1–55.
54. Vermeesch, P. IsoplotR: A free and open toolbox for geochronology. *Geosci. Front.* **2018**, *9*, 1479–1493. [[CrossRef](#)]
55. Ma, Q.; Zheng, J.P.; Griffin, W.L.; Zhang, M.; Tang, H.Y.; Su, Y.P.; Ping, X.P. Triassic “Ada-kitic” Rocks in an Extensional Setting (North China): Melts from the Cratonic Lower Crust. *Lithos* **2012**, *149*, 159–173. [[CrossRef](#)]
56. Belousova, E.A.; Griffin, W.L.; O’Reilly, S.Y.; Fisher, N.I. Igneous zircon: Trace element composition as an indicator of source rock type. *Contrib. Mineral. Petrol.* **2002**, *143*, 602–622. [[CrossRef](#)]
57. Wu, Y.B.; Zheng, Y.F. Genesis of zircon and its constraints on interpretation of U-Pb age. *Chin. Sci. Bull.* **2004**, *49*, 1554–1569. [[CrossRef](#)]
58. Siebel, W.; Blaha, U.; Chen, F.; Rohrmüller, J. Geochronology and geochemistry of a dyke–host rock association and implications for the formation of the Bavarian Pfahl shear zone, Bohemian Massif. *Int. J. Earth Sci.* **2005**, *94*, 8–23. [[CrossRef](#)]
59. Middlemost, E.A.K. Naming materials in the magma/igneous rock system. *Earth-Sci. Rev.* **1994**, *37*, 215–224. [[CrossRef](#)]
60. Rickwood, P.C. Boundary lines within petrologic diagrams which use oxides of major and minor elements. *Lithos* **1989**, *22*, 247–263. [[CrossRef](#)]
61. Frost, C.D.; Frost, B.R. On ferroan (A-type) granitoids: Their compositional variability and modes of origin. *J. Pet.* **2010**, *52*, 39–53. [[CrossRef](#)]
62. Maniar, P.D.; Piccoli, P.M. Tectonic discrimination of granitoids. *Geol. Soc. Am. Bull.* **1989**, *101*, 635–643. [[CrossRef](#)]
63. Sun, S.S.; McDonough, W.F. Chemical and isotopic systematics of oceanic basalts: Implications for mantle composition and processes. *Geol. Soc. Lond. Spec. Publ.* **1989**, *42*, 313–345. [[CrossRef](#)]
64. Sylvester, P.J. Post-collisional strongly peraluminous granites. *Lithos* **1998**, *45*, 29–44. [[CrossRef](#)]
65. Bonin, B.; Sekkal, A.A.; Bussy, F.; Ferrag, S. Alkali-calcic and alkaline post-orogenic granite magmatism: Petrologic constraints and geodynamic settings. *Lithos* **1998**, *45*, 45–70. [[CrossRef](#)]
66. Huang, W.L.; Wyllie, P.J. Phase relationships of S-type granite with H<sub>2</sub>O to 35 kbar: Muscovite granite from Harney Peak, South Dakota. *J. Geophys. Res.* **1981**, *86*, 10515–10529. [[CrossRef](#)]
67. Lubala, R.T.; Frick, C.; Roders, J.H.; Walraven, F. Petro-genesis of syenites and granites of the Schiel Alkaline complex, Northern Transvaal, South Africa. *J. Geol.* **1994**, *102*, 307–309. [[CrossRef](#)]
68. Brown, P.E.; Becker, S.M. Fractionation, hybridisation and magma-mixing in the Kialineq centre East Greenland. *Contrib. Miner. Pet.* **1986**, *92*, 57–70. [[CrossRef](#)]
69. Lynch, D.J.; Musselman, T.E.; Gutmann, J.T.; Patchett, P.J. Isotopic evidence for the origin of Cenozoic volcanic rocks in the Pinacate volcanic field, northwestern Mexico. *Lithos* **1993**, *29*, 295–302. [[CrossRef](#)]
70. Yang, J.H.; Chung, S.L.; Wilde, S.A.; Wu, F.; Chu, M.F.; Lo, C.H.; Fan, H.R. Petrogenesis of post-orogenic syenites in the Sulu Orogenic Belt, East China: Geochronological, geochemical and Nd–Sr isotopic evidence. *Chem. Geol.* **2005**, *214*, 99–125. [[CrossRef](#)]
71. Dorais, M.J. Compositional variations in pyroxenes and amphiboles of the Belknap Mountain complex, New Hampshire: Evidence for origin of silica-saturated alkaline rocks. *Am. Miner.* **1990**, *75*, 1092–1105.
72. Litvinovsky, B.A.; Jahn, B.M.; Zanzvilevich, A.N.; Shadaev, M.G. Crystal fractionation in the petrogenesis of an alkali monzodiorite-syenite series: The Oshurkovo plutonic sheeted complex, Transbaikalia, Russia. *Lithos* **2002**, *64*, 97–130. [[CrossRef](#)]
73. Qin, J.F.; Lai, S.C.; Grapes, R.; Diwu, C.R.; Ju, Y.J.; Li, Y.F. Origin of Late Triassic high-Mgadakitic granitoid rocks from the Dongjiangkou area, Qinling orogen, Central China implications for subduction of continental crust. *Lithos* **2010**, *120*, 347–367. [[CrossRef](#)]
74. Stern, R.J. Subduction zones. *Rev. Geophys.* **2002**, *40*, 1012. [[CrossRef](#)]
75. Zhang, H.; Hou, Z.; Yang, T.; Song, Y.; Li, Z.; Wang, Z.; Wang, Y.; Liu, Q. Subduction-related Quartz. Syenite Porphyries in the Eastern Qiangtang Terrane, Qinghai-Tibet Plateau: Constraints from geochemical analyses. *Geol. Rev.* **2010**, *56*, 405–414. (In Chinese with English abstract)
76. Deng, J.F.; Zhao, H.L.; Luo, Z.H.; Guo, Z.F.; Mo, X.X. Mantle plumes and lithosphere motion in East Asia. In *Mantle Dynamics and Plate Interactions in East Asia*; Flower, M.F.J., Chung, S.L., Lo, C.H., Lee, T.Y., Eds.; American Geophysical Union: Washington, DC, USA, 1998; pp. 59–65.
77. Deng, J.F.; Qiu, R.Z.; Xiao, Q.H.; Wu, Z.X.; Zhou, S.; Peng, C.; Zhao, G.C.; SU, S.G.; Liu, C. Input of Material and Heat from Convective Mantle into Continent and Continental Metallogensis. *Miner. Depos.* **2004**, *23*, 24–31, (In Chinese with English abstract).
78. Litvinovsky, B.A.; Steele, I.M.; Wickham, S.M. Silicic magma formation in overthickened crust: Melting of charnockite and leucogranite at 15, 20 and 25 kbar. *J. Petrol.* **2000**, *41*, 717–737. [[CrossRef](#)]

79. Xiao, Q.H.; Deng, J.F.; Qiu, R.Z.; Liu, Y.; Feng, Y.F. A preliminary study of the relationship between granitoids and the growth of continental crust: A case study of the formation of key orogen granitoids in China. *Geol. China* **2009**, *36*, 594–622. (In Chinese with English abstract)
80. Long, X.P.; Sun, M.; Yuan, C.; Xiao, W.J.; Lin, S.F.; Wu, F.Y.; Xia, X.P.; Cai, K.D. Detrital zircon age and Hf isotopic studies for meta sedimentary rocks from the Chinese Altai: Implications for the Early Paleozoic tectonic evolution of the Central Asian Orogenic Belt. *Tectonics* **2007**, *26*, TC5015. [[CrossRef](#)]
81. Pei, X.Z.; Li, Z.C.; Ding, S.P.; Li, Y.; Hu, B.; Liu, H.B. Geochemical characteristics and zircon U-Pb ages of island-arc basic igneous complexes in the Tianshui area, West Qinling. *Geol. China* **2005**, *4*, 5–16. (In Chinese with English abstract) [[CrossRef](#)]
82. Ding, S.P.; Pei, X.Z.; Hu, B.; Li, Y.; Guo, J.F.; Li, Z.C.; Zhao, X. Geochemical Characteristics and Origin of Cenozoic Acid Volcanic Rocks in the TianShui area Gansu province. *Geol. Prospect.* **2005**, *1*, 33–37. (In Chinese with English abstract)
83. Xu, L.L.; Bi, X.W.; Su, W.C.; Hu, R.Z.; Tang, Y. Geochemical characteristics and petrogenesis of the quartz syenite porphyry from Tongchang porphyry Cu(Mo-Au) deposit in Jinping County, Yunnan Province. *Acta Petrol. Sin.* **2011**, *27*, 3109–3122.
84. Li, L.; Meng, Q.R.; Pullen, A.; Garzzone, C.N.; Wu, G.L.; Wang, Y.L.; Ma, S.X.; Duan, L. Late Permian-Early Middle Triassic back-arc basin development in West Qinling, China. *J. Asian Earth Sci.* **2014**, *87*, 116–129. [[CrossRef](#)]
85. Hou, Z.Q.; Qu, X.M.; Yang, Z.S.; Meng, X.J.; Li, Z.Q.; Yang, Z.M.; Zheng, M.P.; Zheng, Y.Y.; Nie, F.J.; Gao, Y.F.; et al. Metallogenesis in Tibetan collisional orogenic belt: III. Mineralization in post-collisional extension setting. *Miner. Depos.* **2006**, *6*, 629–651. (In Chinese with English abstract).
86. Zhao, Z.H.; Xiong, X.L.; Wang, Q.; Qiao, Y.L. Some aspects on geochemistry of Nb and Ta. *Geochemistry.* **2019**, *44*, 4203–4221. (In Chinese with English abstract).
87. Jia, X.H.; Wang, Q.; Tan, G.J. A-type Granites: Research Progress and Implications. *Geotecton. Metallog.* **2009**, *33*, 465–480. (In Chinese with English abstract).
88. Sun, W.; Li, S.; Chen, Y.; Li, Y. Timing of synorogenic granitoids in the south Qinling, central China: Constraints on the evolution of the Qinling-Dabie orogenic belt. *J. Geol.* **2002**, *110*, 457–468. [[CrossRef](#)]
89. Zhang, C.L.; Wang, T.; Wang, X.X. Genesis and tectonic setting of early Mesozoic granites in the Qinling Orogenic belt. *Geol. J. China Univ.* **2008**, *53*, 304–316. (In Chinese with English abstract)
90. Ji, S.; Li, Z.C.; Pei, X.Z.; Pei, L.; Li, R.B.; Liu, C.J.; Chen, Y.X.; Lin, H.; Wang, M. Petrogenesis and Tectonic Significance of Late Triassic A1-Type Granite from the West Section of North Qinling Orogenic Belt: Constraints from Geochronology and Geochemistry. *Minerals* **2023**, *13*, 557. [[CrossRef](#)]
91. Gong, X.K.; Chen, D.L.; Zhu, X.H.; Dong, Z.C.; Guo, C.L. The determination of Triassic ultramafic-syenite intrusive body and its geological significance, western North Qinling. *Acta Petrol. Sin.* **2016**, *32*, 177–192. (In Chinese with English abstract)
92. Zhu, L.M.; Ding, Z.J.; Yao, S.Z.; Zhang, G.W.; Song, S.M.; Qu, W.J.; Guo, B.; Li, B. Metallogenic Geological Events and Metallogenic Tectonic Background of the Wenquan Molybdenum Deposit in Gansu, West Qinling Mountains. *Sci. Bull.* **2009**, *54*, 2337–2347+2439–2441. (In Chinese)
93. Li, Z.C.; Pei, X.Z.; Li, R.B.; Pei, L.; Hu, B.; Liu, C.J.; Chen, G.C.; Chen, Y.X. LA-ICP-MS zircon U-Pb dating, geochemistry of the Mishuling intrusion in western Qinling and their tectonic significance. *Acta Petrol. Sin.* **2013**, *29*, 2617–2634. (In Chinese with English abstract)
94. Pearce, J.A.; Harris, N.; Tindle, A.G. Trace Element Discrimination Diagrams for the Tectonic Interpretation of Granitic Rocks. *J. Pet.* **1984**, *25*, 956–983. [[CrossRef](#)]
95. Clemens, J.D.; Holloway, J.R.; White, A.J.R. Origin of an A-type granite: Experimental constraints. *Am. Mineral.* **1986**, *71*, 317–324.
96. Hong, D.W.; Wang, S.G.; Han, B.F.; Jin, M.Y. Classification and identification criteria of tectonic environment of alkaline granite. *Sci. China* **1995**, *4*, 418–426. (In Chinese)
97. Douce, A.E.P. Generation of metaluminous A-type granites by low-pressure melting of calc-alkaline granitoids. *Geology* **1997**, *25*, 743–746. [[CrossRef](#)]
98. Dall’Agnol, R.; Brazil, B.P.; Frost, C.D.; Rämö, O.T. IGCP Project 510 “A-type Granites and Related Rocks through Time”: Project vita, results, and contribution to granite research. *Lithos* **2012**, *151*, 1–16. [[CrossRef](#)]
99. Zhang, B.R. Magmatic Activity from source in the Qinling Orogenic belt and Its Dynamic Significance. *Earth Sci. Front.* **2001**, *3*, 57–66. (In Chinese with English abstract)
100. Zhou, W.G.; Zhang, B.R.; Yang, W.R.; Zhao, Z.D.; Xie, H.S. Geochemical characteristics and tectonic Implications of post collision intermediate acid volcanic rocks from Qinling Dabie Orogen. *Geochemistry* **1998**, *6*, 537–548. (In Chinese with English abstract)
101. Zhang, H.F.; Luo, T.C.; Zhang, B.R. The Source Characteristics and Tectonic Environment of the Piaochi batholith in the North Qinling. *Geol. Rev.* **1996**, *3*, 209–214. (In Chinese with English abstract)
102. Zhang, H.F.; Ouyang, J.P.; Lin, W.L. Pb, Sr, Nd Isotope Composition of Ningshan Granitoids, South Qinling and their Deep Geological Information. *J. Mineral.* **1997**, *1*, 23–26+28–33. (In Chinese with English abstract)
103. Jiang, Y.H.; Jin, G.D.; Liao, S.Y.; Zhou, Q.; Zhao, P. Geochemical and Sr–Nd–Hf isotopic constraints on the origin of Late Triassic granitoids from the Qinling orogen, central China: Implications for a continental arc to continent–continent collision. *Lithos* **2010**, *117*, 183–197. [[CrossRef](#)]
104. Kong, J.; Niu, Y.; Duan, M.; Zhang, Y.; Hu, Y.; Li, J.; Chen, S. Petrogenesis of Luchubaand Wuchaba granitoids in western Qinling: Geochronological and geochemical evidence. *Mineral. Petrol.* **2017**, *111*, 887–908. [[CrossRef](#)]
105. Patino Douce, A.E.; Harris, N. Experimental constraints on Himalaya anatexis. *J. Petrol.* **1998**, *39*, 689–710. [[CrossRef](#)]

106. Ferry, J.M.; Watson, E.B. New thermodynamic models and revised calibrations for the Ti-in-zircon and Zr-in-rutile thermometers. *Contrib. Mineral. Petrol.* **2007**, *154*, 429–437. [[CrossRef](#)]
107. Liang, W.T. *Intracontinental Structural Characteristics and Evolution of the Transition Zone between the Eastern and Western Qin ling Mountains in the Qinling Orogenic Belt Process of Transformation*; Xi'an Northwest University: Xi'an, China, 2009; pp. 155–157.
108. Feng, Y.M.; Cao, X.D.; Zhang, E.P.; Hu, Y.X.; Pan, X.P.; Yang, J.L.; Jia, Q.Z.; Li, W.M. Evolution Structural Patterns and Properties of the Western Qinling Orogenic Belt. *Northwest. Geol.* **2003**, *36*, 1.

**Disclaimer/Publisher's Note:** The statements, opinions and data contained in all publications are solely those of the individual author(s) and contributor(s) and not of MDPI and/or the editor(s). MDPI and/or the editor(s) disclaim responsibility for any injury to people or property resulting from any ideas, methods, instructions or products referred to in the content.